Supporting Information: Revisiting the Θ Point

Pengfei Zhang,[†,‡] Nayef M. Alsaifi,[¶] and Zhen-Gang Wang[*,‡]

†*Center for Advanced Low-Dimension Materials, State Key Laboratory for Modification of Chemical Fibers and Polymer Materials, Donghua University, Shanghai 201620, China*

‡*Division of Chemistry and Chemical Engineering, California Institute of Technology, Pasadena, CA 91125, United States*

¶*Chemical Engineering Department, King Fahd University of Petroleum & Minerals, Dhahran, Saudi Arabia*

E-mail: zgw@caltech.edu

S1. Derivation of B_2 within the first-order perturbation theory

As mentioned in the main text, the contributions to B_2 due to the second virial interaction and the square gradient interaction are $B_{2,v} = v/2$ and 0 respectively. The contribution due

to the three-body interaction is derived as follows:

$$
\begin{aligned}
B_{2,w} &= 2\frac{V}{2N^2}\frac{w}{V^2}\sum_{s=1}^{N-1}\sum_{s'=s+1}^{N}\sum_{t=1}^{N}\int \mathrm{d}\mathbf{R}_1\mathrm{d}\mathbf{R}_s\mathrm{d}\mathbf{R}_{s'}\mathrm{d}\mathbf{R}'_1\mathrm{d}\mathbf{R}_2\mathrm{d}\mathbf{R}_t\mathrm{d}\mathbf{R}'_2 \\
&\quad \int \mathrm{d}\mathbf{r}\delta(\mathbf{r}-\mathbf{R}_s)\delta(\mathbf{r}-\mathbf{R}_{s'})\delta(\mathbf{r}-\mathbf{R}_t) \\
&\quad G_0(\mathbf{R}_1,\mathbf{R}_s;s)G_0(\mathbf{R}_s,\mathbf{R}_{s'};s'-s+1)G_0(\mathbf{R}'_s,\mathbf{R}'_1;N-s'+1) \\
&\quad G_0(\mathbf{R}_2,\mathbf{R}_t;t)G_0(\mathbf{R}_t,\mathbf{R}'_2;N-t+1) \\
&= \frac{w}{VN^2}\sum_{s=1}^{N-1}\sum_{s'=s+1}^{N}\sum_{t=1}^{N}\int \mathrm{d}\mathbf{R}_1\mathrm{d}\mathbf{R}'_1\mathrm{d}\mathbf{R}_2\mathrm{d}\mathbf{R}'_2\int \mathrm{d}\mathbf{r}G_0(\mathbf{R}_1,\mathbf{r};s)G_0(\mathbf{r},\mathbf{r};s'-s+1) \\
&\quad G_0(\mathbf{r},\mathbf{R}'_1;N-s'+1)G_0(\mathbf{R}_2,\mathbf{r};t)G_0(\mathbf{r},\mathbf{R}'_2;N-t+1) \\
&= \frac{w}{N}\sum_{s=1}^{N-1}\sum_{s'=s+1}^{N}\left[\frac{3}{2\pi(s'-s)b^2}\right]^{3/2} \\
&= \frac{w}{Nb^3}\left(\frac{3}{2\pi}\right)^{3/2}\sum_{t=1}^{N-1}(N-t)t^{-3/2}
\end{aligned}
\tag{S1}
$$

where we have used the propagator

$$
G_0(\mathbf{r},\mathbf{r}';N) = \left[\frac{3}{2\pi(N-1)b^2}\right]^{3/2}\exp\left[-\frac{3(\mathbf{r}-\mathbf{r}')^2}{2(N-1)b^2}\right] \tag{S2}
$$

which represents the probability for a given chain consisting of N monomers starting at $\mathbf{r}$ and ending at $\mathbf{r}'$.

S2. Diagrams used to calculate the first-order correction of $\left\langle R_e^2\right\rangle$ and $\left\langle R_g^2\right\rangle$

The first-order correction to the mean-square chain end-to-end distance can be schematically represented by Fig. S1, where the black line denotes the propagator along the chain contour and the red dash represents the interaction. Specifically, the dash in Fig. S1(a) represents either the second virial interaction or the square gradient interaction, while that in Fig. S1(b)

represents the third virial interaction.

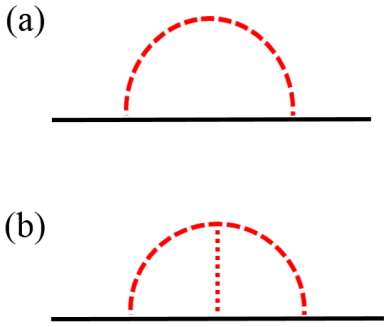

Figure S1: Feynman diagrams involved in the calculation of $\delta\langle R_e^2\rangle$ defined in Eq.(31). Part (a) accounts for contributions from v and κ. Part (b) represents that from w.

On the other hand, $\delta\langle R_g^2\rangle \equiv N^{-2}\sum_{i=1}^{N-1}\sum_{j=i+1}^{N}\delta\langle R_e^2(i,j)\rangle$, and $\delta\langle R_e^2(i,j)\rangle$ is schematically represented by Fig. S2, where i and j denote the positions of the i-th and j-th monomers on the chain contour. In Sec. S3, we will take one example to illustrate how to calculate $\delta\langle R_e^2\rangle$ and $\delta\langle R_e^2(i,j)\rangle$ using the diagrams shown in Figs. S1 and S2.

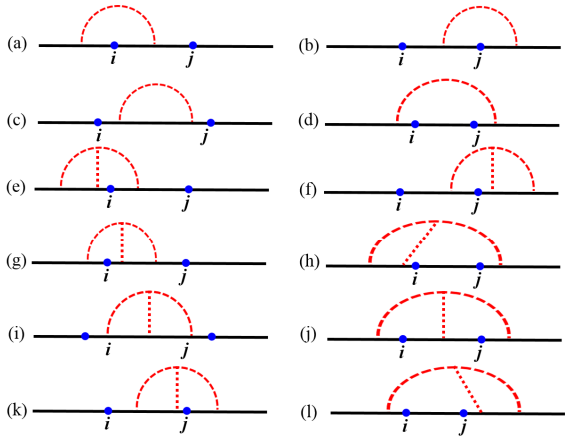

Figure S2: Feynman diagrams involved in the calculation of $\delta R_e^2(i,j;N)$ for a partial chain starting from the i-th segment and ending at the j-th segment. Parts (a)-(d) account for contributions from the monomer second virial interaction and the square-gradient interaction. Parts (e)-(l) represent those from the third virial interaction.

S3. Contribution due to Part (j) of Fig. S2

Taking part (j) of Fig. (S2) as an example, we illustrate how to calculate $\delta\left\langle R_e^2(i,j;N)\right\rangle$ and $\delta\left\langle R_g^2\right\rangle$. Part (j) of Fig. (S2) denotes one part of $\delta\left\langle R_e^2(i,j;N)\right\rangle$ due to w; the black line denotes the polymer chain and the red dashed curve denotes the three-body interaction. Note that the figure depicts only the topology of the chain backbone along with the relavent interactions instead of the actual spatial positions of segments. We label the left and right ends of the black line as 1 and N, and the three intersecting points between the black line and the red curves from the left to the right as s, t and l respectively. These points thus denote the 1-st, s-th, t-th, l-th and N-th monomers along the backbone. The s-th, t-th, l-th monomers as well as the pre-specified i-th and j-th monomers divide the whole chain into six sections. In the following, we further denote the spatial positions of the 1-st, s-th, t-th, l-th, N-th monomers as well as the pre-specified i-th and j-th monomers as $\mathbf{R}_1$, $\mathbf{R}_s$, $\mathbf{R}_t$, $\mathbf{R}_l$, $\mathbf{R}_N$, $\mathbf{R}_i$ and $\mathbf{R}_j$ respectively. Since there are two terms in $\delta R_e^2(i,j;N)$ (see the general expression given in Eq. (11) of the main text), we derive them separately. The corresponding contribution to the first term $\left\langle\beta\mathcal{H}_{nb}R_e^2(i,j;N)\right\rangle_0$ is

$$
\begin{aligned}
X_w &= \frac{w}{V}\sum_{s=1}^{i-1}\sum_{t=i}^{j-1}\sum_{l=j}^{N}\int \mathrm{d}\mathbf{R}_1\mathrm{d}\mathbf{R}_s\mathrm{d}\mathbf{R}_i\mathrm{d}\mathbf{R}_t\mathrm{d}\mathbf{R}_j\mathrm{d}\mathbf{R}_l\mathrm{d}\mathbf{R}_N G_0(\mathbf{R}_1,\mathbf{R}_s;s)G_0(\mathbf{R}_s,\mathbf{R}_i;i-s+1)\\
&\quad G_0(\mathbf{R}_i,\mathbf{R}_t;t-i+1)G_0(\mathbf{R}_t,\mathbf{R}_j;j-t+1)G_0(\mathbf{R}_j,\mathbf{R}_l;l-j+1)G_0(\mathbf{R}_l,\mathbf{R}_N;N-l+1)\\
&\quad \delta(\mathbf{R}_s-\mathbf{R}_t)\delta(\mathbf{R}_t-\mathbf{R}_l)(\mathbf{R}_i-\mathbf{R}_j)^2\\
&= w\sum_{s=1}^{i-1}\sum_{t=i}^{j-1}\sum_{l=j}^{N}\int \mathrm{d}\mathbf{R}_i\mathrm{d}\mathbf{R}_j G_0(\mathbf{0},\mathbf{R}_i;i-s+1)G_0(\mathbf{R}_i,\mathbf{0};t-i+1)G_0(\mathbf{0},\mathbf{R}_j;j-t+1)\\
&\quad G_0(\mathbf{R}_j,\mathbf{0};l-j+1)(\mathbf{R}_i^2+\mathbf{R}_j^2)\\
&= \frac{w}{b^4}\left(\frac{3}{2\pi}\right)^3\sum_{s=1}^{i-1}\sum_{t=i}^{j-1}\sum_{l=j}^{N}\left[\frac{(i-s)(t-i)}{(t-s)^{5/2}(l-t)^{3/2}}+\frac{(j-t)(l-j)}{(l-t)^{5/2}(t-s)^{3/2}}\right];
\end{aligned}
\tag{S3}
$$

on the other hand, the corresponding contribution to $\langle \beta \mathcal{H}_{nb} \rangle_0$ in the second term is

$$\begin{aligned} Y_w &= \frac{w}{V} \sum_{s=1}^{i-1} \sum_{t=i}^{j-1} \sum_{l=j}^{N} \int \mathrm{d}\mathbf{R}_1 \mathrm{d}\mathbf{R}_s \mathrm{d}\mathbf{R}_i \mathrm{d}\mathbf{R}_t \mathrm{d}\mathbf{R}_j \mathrm{d}\mathbf{R}_l \mathrm{d}\mathbf{R}_N G_0(\mathbf{R}_1, \mathbf{R}_s; s) G_0(\mathbf{R}_s, \mathbf{R}_i; i-s+1) \\ & \quad G_0(\mathbf{R}_i, \mathbf{R}_t; t-i+1) G_0(\mathbf{R}_t, \mathbf{R}_j; j-t+1) G_0(\mathbf{R}_j, \mathbf{R}_l; l-j+1) G_0(\mathbf{R}_l, \mathbf{R}_N; N-l+1) \\ & \quad \delta(\mathbf{R}_s - \mathbf{R}_t) \delta(\mathbf{R}_t - \mathbf{R}_l) \\ &= \frac{w}{b^6} \left(\frac{3}{2\pi} \right)^3 \sum_{s=1}^{i-1} \sum_{t=i}^{j-1} \sum_{l=j}^{N} \frac{1}{(t-s)^{3/2} (l-t)^{3/2}}, \end{aligned} \tag{S4}$$

and finally we have the corresponding contribution to $\delta \langle R_e^2(i,j;N) \rangle$ from Part (j) of the Feynman diagrams as

$$Z_w(i,j;N) \equiv Y_w (j-i) b^2 - X_w = \sum_{s=i}^{j-2} \sum_{t=s+1}^{j-1} \sum_{l=j+1}^{N} \frac{(j-s)(l-t) - (l-j)(j-t)}{(t-s)^{3/2} (l-t)^{5/2}}; \tag{S5}$$

where we have used Eq. (S2).

S4. Expression for $\delta \left\langle R_e^2(i,j;N) \right\rangle$ from the first-order perturbation theory

By following the same procedure as shown in Sec. S3, we calculate all 16 contributions (4 for v, 4 for κ, and 8 for w), and the final expression for $\delta \langle R_e^2(i,j;N) \rangle$ is given by

$$\delta \left\langle R_e^2(i,j;N) \right\rangle = \frac{v}{b} \left(\frac{3}{2\pi} \right)^{3/2} T_v'(i,j;N) + \frac{15\kappa}{b^3} \left(\frac{3}{2\pi} \right)^{3/2} T_\kappa'(i,j;N) + \frac{w}{b^4} \left(\frac{3}{2\pi} \right)^3 T_w'(i,j;N), \tag{S6}$$

where

$$T_v'(i,j;N) \equiv \sum_{s=1}^{i} \sum_{t=i+1}^{j} \frac{(t-i)^2}{(t-s)^{5/2}} + \sum_{s=1}^{i} \sum_{t=j+1}^{N} \frac{(j-i)^2}{(t-s)^{5/2}} + \sum_{s=i+1}^{j-1} \sum_{t=s+1}^{j} \frac{1}{(t-s)^{1/2}} + \sum_{s=i+1}^{j-1} \sum_{t=j+1}^{N} \frac{(s-j)^2}{(t-s)^{5/2}} \tag{S7}$$

$$T'_{\kappa}(i,j;N) \equiv \sum_{s=1}^{i}\sum_{t=i+1}^{j}\frac{(t-i)^2}{(t-s)^{7/2}}+\sum_{s=1}^{i}\sum_{t=j+1}^{N}\frac{(j-i)^2}{(t-s)^{7/2}}+\sum_{s=i+1}^{j-1}\sum_{t=s+1}^{j}\frac{1}{(t-s)^{3/2}}+\sum_{s=i+1}^{j-1}\sum_{t=j+1}^{N}\frac{(s-j)^2}{(t-s)^{7/2}} \tag{S8}$$

and

$$\begin{aligned}
T'_{w}(i,j;N) \equiv & \sum_{s=1}^{i-1}\sum_{t=s+1}^{i}\sum_{l=i+1}^{j}\frac{(l-i)^2}{(l-t)^{5/2}(t-s)^{3/2}}+\sum_{s=1}^{i-1}\sum_{t=s+1}^{i}\sum_{l=j+1}^{N}\frac{(j-i)^2}{(l-t)^{5/2}(t-s)^{3/2}} \\
& + \sum_{s=1}^{i-1}\sum_{t=i+1}^{j-1}\sum_{l=t+1}^{j}\frac{(l-i)(t-s)-(i-s)(t-i)}{(t-s)^{5/2}(l-t)^{3/2}} \\
& + \sum_{s=1}^{i-1}\sum_{t=i+1}^{j-1}\sum_{l=j+1}^{N}\frac{(j-i)(l-t)(t-s)-(i-s)(t-i)(l-t)-(j-t)(l-j)(t-s)}{(t-s)^{5/2}(l-t)^{5/2}} \\
& + \sum_{s=1}^{i-1}\sum_{t=j}^{N-1}\sum_{l=t+1}^{N}\frac{(j-i)^2}{(t-s)^{5/2}(l-t)^{3/2}}+\sum_{s=i}^{j-2}\sum_{t=s+1}^{j-1}\sum_{l=t+1}^{j}\frac{l-s}{(t-s)^{3/2}(l-t)^{3/2}} \\
& + \sum_{s=i}^{j-2}\sum_{t=s+1}^{j-1}\sum_{l=j+1}^{N}\frac{(j-s)(l-t)-(l-j)(j-t)}{(t-s)^{3/2}(l-t)^{5/2}}+\sum_{s=i}^{j-1}\sum_{t=j}^{N-1}\sum_{l=t+1}^{N}\frac{(j-s)^2}{(t-s)^{5/2}(l-t)^{3/2}}.
\end{aligned} \tag{S9}$$

S5. Comparison between discrete Gaussian chain (DGC) and continuous Gaussian chain (CGC) models

In the main text, we have presented the results for the DGC model; here we will compare them with results of the CGC model with a highlight on their differences. We note that in previous works,[S1–S4] either only the w term or the κ term is included to examine the respective influence on the Θ point, here we take into account both w and κ terms. First, the Θ point for the CGC model, as derived in Eq. (23) of the main text, is given by

$$v_{\Theta_N} \approx \frac{2w}{b^3}\left(\frac{3}{2\pi}\right)^{3/2}\left[-2s_0^{-1/2}+\frac{4}{\sqrt{N}}\right] = v_{\Theta_\infty}+\frac{8w}{b^3}\left(\frac{3}{2\pi}\right)^{3/2}N^{-1/2}, \tag{S10}$$

where the expression of v_{Θ_∞} is self-evident and s_0 is a microscopic cutoff whose value is arbitrary. Since v_{Θ_∞} explicitly depends on s_0, it is not well-defined in the CGC model, unlike in the DGC model. The leading order corrections (i.e., $O(N^{-1/2})$) for both models, however, are the same.

On the other hand, at Θ_∞, the leading order corrections to $\delta\left\langle R_e^2\right\rangle$ and $\delta\left\langle R_g^2\right\rangle$ are, respectively,

$$\begin{aligned}\delta\left\langle R_e^2\right\rangle(\Theta_\infty) &= \frac{30\kappa}{b^3}\left(\frac{3}{2\pi}\right)^{3/2} N s_0^{-1/2} - \left(\frac{3}{2\pi}\right)^3 \frac{w}{b^4} 4\pi N \\ &\approx \left(9.8977\frac{\kappa}{b^3}s_0^{-1/2} - 1.3678\frac{w}{b^4}\right) N, \end{aligned} \tag{S11}$$

and

$$\begin{aligned}\delta\left\langle R_g^2\right\rangle(\Theta_\infty) &= \frac{5\kappa}{b^3}\left(\frac{3}{2\pi}\right)^{3/2} N s_0^{-1/2} - \frac{Nb^2}{6}\left(\frac{3}{2\pi}\right)^3 \frac{w}{b^6}\frac{13\pi}{4} \\ &\approx \left(1.6496\frac{\kappa}{b^3}s_0^{-1/2} - 0.1852\frac{w}{b^4}\right) N. \end{aligned} \tag{S12}$$

Likewise, at Θ_N, the $N^{3/2}$ term vanishes and we have

$$\begin{aligned}\delta\left\langle R_e^2\right\rangle(\Theta_N) &= \frac{30\kappa}{b^3}\left(\frac{3}{2\pi}\right)^{3/2} N s_0^{-1/2} - \left(\frac{3}{2\pi}\right)^3 \left(4\pi - \frac{32}{3}\right) \frac{w}{b^4} N \\ &\approx \left(9.8977\frac{\kappa}{b^3}s_0^{-1/2} - 0.2068\frac{w}{b^4}\right) N, \end{aligned} \tag{S13}$$

and

$$\begin{aligned}\delta\left\langle R_g^2\right\rangle(\Theta_N) &= \frac{5\kappa}{b^3}\left(\frac{3}{2\pi}\right)^{3/2} N s_0^{-1/2} - \frac{Nb^2}{6}\left(\frac{3}{2\pi}\right)^3 \frac{w}{b^6}\left(\frac{13\pi}{4} - \frac{134\times 8}{105}\right) \\ &\approx \left(1.6496\frac{\kappa}{b^3}s_0^{-1/2} - 1.183\times 10^{-5}\frac{w}{b^4}\right) N. \end{aligned} \tag{S14}$$

where the w terms are adopted from Ref. [S2]; in the second line of these four equations, we have substituted the numerical values to obtain explicit expressions. On the other hand, we

are unable to obtain the w coefficient of the subleading $O(N^{1/2})$ correction to both $\langle R_e^2 \rangle$ and $\langle R_g^2 \rangle$ at Θ_N and Θ_∞ is unknown (no report in literature also to the best of our knowledge); however, the κ part of the $O(N^{1/2})$ correction can be easily obtained as $-60[3/(2\pi)]^{3/2}\kappa/b^3 \approx -19.7954\kappa/b^3$ for $\langle R_e^2 \rangle$ at Θ_N and Θ_∞, and $-(31/3)[3/(2\pi)]^{3/2}\kappa/b^3 \approx -3.4092\kappa/b^3$ for $\langle R_g^2 \rangle$ at Θ_N and Θ_∞ respectively.

These expressions can be quantitatively compared with the DGC results given by Table 2 of the main text. In particular, we see the w coefficient of the $O(N)$ term and the κ coefficient of the $O(N^{1/2})$ terms are approximately the same in CGC and DGC models for all quantities. We regard the slight difference (if any) as due to the numerical errors when evaluating the coefficient in DGC. Thus, the dimensional regularization and cutoff schemes commonly used in the CGC model[S2] and our treatment for the DGC model are equivalent up to the $O(N)$ order correction for the three-parameter model. Furthermore, since the κ coefficient of the $O(N)$ term for the CGC models depends on s_0 explicitly, it is impossible to compare the chain sizes at Θ_N and Θ_∞ with the ideal chain with *bare* Kuhn length b for finite κ and it is necessary to introduce a renormalized Kuhn length b_r[S5] via

$$b_r^2 \equiv b^2 + \frac{30\kappa}{b^3}\left(\frac{3}{2\pi}\right)^{3/2} s_0^{-1/2}. \tag{S15}$$

Therefore, at Θ_∞, both $\langle R_e^2 \rangle$ and $\langle R_g^2 \rangle$ are contracted with an $O(N)$ leading-order correction when comparing with the ideal chain size with b_r. On the other hand, at Θ_N, while $\langle R_e^2 \rangle$ is also contracted with an $O(N)$ leading-order correction, that of $\langle R_g^2 \rangle$ should be on $O(N^{1/2})$ due to the w coefficient of the $O(N)$ term being negligibly small, but we cannot determine the sign of the $O(N^{1/2})$ term due to the lack of the knowledge of the w coefficient of this correction.

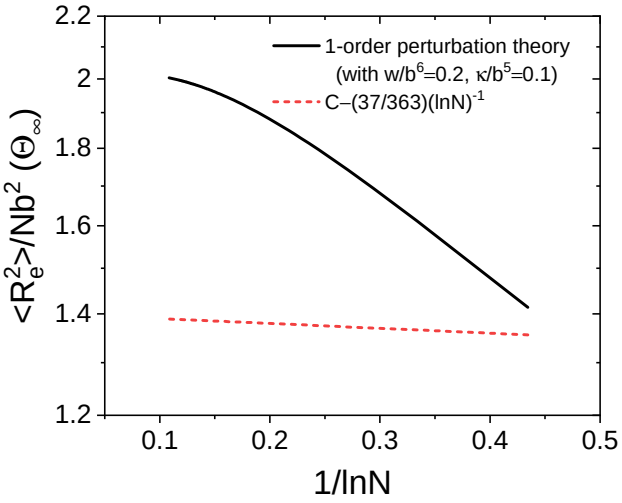

Figure S3: The N dependence of $R_e^2(\Theta_\infty)/Nb^2$ from our first-order perturbation calculation with $w/b^6 = 0.2$ and $\kappa/b^5 = 0.1$, and that from the RG calculation.[S2]

S6. Qualitative explanation of Monte Carlo simulation results using first-order perturbation theory

As mentioned in the Introduction of the main text, Grassberger and Hegger[S6] performed systematic lattice Monte Carlo (MC) simulation to check the applicability of the logarithmic correction in various quantities such as $\langle R_e^2 \rangle$ and $\langle R_g^2 \rangle$ at Θ_∞ as predicted by the renormalization group (RG) calculation by Duplantier.[S2,S7] In particular, they found that the amplitude of the corrections in MC simulations is much larger than the universal amplitude of the leading logarithmic corrections;[S2] this difference was later explained by Hagar and Schäfer who argued that the subleading correction is equally important when explaining the MC results for the chain length studied.[S8]

Our first-order perturbation theory provides an alternative perspective on understanding these MC results. In Fig. S3 we show the N dependence of $\langle R_e^2 \rangle (\Theta_\infty)/Nb^2$ obtained using Eq. (41) with $\kappa/b^5 = 0.1$ and $w/b^6 = 0.2$; we also include the RG prediction[S2] for comparison. We see the N dependence of our first-order perturbation result is much stronger than the logarithmic correction predicted by the RG theory, and is qualitatively consistent with

the MC results by Grassberger and Hegger (see Fig. 18 in Ref. S6). While a quantitative comparison cannot be made here due to the model difference between these two studies, the qualitatively consistent feature with increasing N in both studies may suggest the importance the κ interaction and the necessity to keep the subleading $O(N^{1/2})$ in $\langle R_e^2 \rangle$ and $\langle R_g^2 \rangle$ at the Θ point when explaining the computer simulation results.

References

(S1) Cherayil, B. J.; Douglas, J. F.; Freed, K. F. Effect of Residual Interactions on Polymer Properties near the Theta Point. *The Journal of Chemical Physics* **1985**, *83*, 5293–5310.

(S2) Duplantier, B. Geometry of Polymer Chains near the Theta-Point and Dimensional Regularization. *The Journal of Chemical Physics* **1987**, *86*, 4233–4244.

(S3) Grosberg, A. Y.; Kuznetsov, D. V. Quantitative Theory of the Globule-to-Coil Transition. 1. Link Density Distribution in a Globule and its Radius of Gyration. *Macromolecules* **1992**, *25*, 1970–1979.

(S4) Shirvanyants, D.; Panyukov, S.; Liao, Q.; Rubinstein, M. Long-Range Correlations in a Polymer Chain Due to Its Connectivity. *Macromolecules* **2008**, *41*, 1475–1485.

(S5) Wang, Z.-G. 50th Anniversary Perspective: Polymer Conformation—A Pedagogical Review. *Macromolecules* **2017**, *50*, 9073–9114.

(S6) Grassberger, P.; Hegger, R. Simulations of Three-Dimensional θ Polymers. *The Journal of Chemical Physics* **1995**, *102*, 6881–6899.

(S7) Duplantier, B. Lagrangian Tricritical Theory of Polymer Chain Solutions near the θ-Point. *Journal de Physique* **1982**, *43*, 991–1019.

(S8) Hager, J.; Schäfer, L. Θ-point behavior of diluted polymer solutions: Can one observe the universal logarithmic corrections predicted by field theory? *Physical Review E* **1999**, *60*, 2071.